JOURNAL OF BACTERIOLOGY, Apr. 2008, p. 2266–2274 Vol. 190, No. 7
0021-9193/08/$08.00+0 doi:10.1128/JB.01841-07

Elucidation of an Alternate Isoleucine Biosynthesis Pathway in *Geobacter sulfurreducens*▽

Carla Risso,[1]* Stephen J. Van Dien,[2] Amber Orloff,[1] Derek R. Lovley,[1] and Maddalena V. Coppi[1]

Department of Microbiology, 203N Morrill Science Center IVN, University of Massachusetts Amherst, Amherst, Massachusetts 01003,[1] and Genomatica, Inc., 5405 Morehouse Drive, Suite 210, San Diego, California 92121[2]

Received 21 November 2007/Accepted 18 January 2008

The central metabolic model for *Geobacter sulfurreducens* included a single pathway for the biosynthesis of isoleucine that was analogous to that of *Escherichia coli*, in which the isoleucine precursor 2-oxobutanoate is generated from threonine. ^{13}C labeling studies performed in *G. sulfurreducens* indicated that this pathway accounted for a minor fraction of isoleucine biosynthesis and that the majority of isoleucine was instead derived from acetyl-coenzyme A and pyruvate, possibly via the citramalate pathway. Genes encoding citramalate synthase (GSU1798), which catalyzes the first dedicated step in the citramalate pathway, and threonine ammonia-lyase (GSU0486), which catalyzes the conversion of threonine to 2-oxobutanoate, were identified and knocked out. Mutants lacking both of these enzymes were auxotrophs for isoleucine, whereas single mutants were capable of growth in the absence of isoleucine. Biochemical characterization of the single mutants revealed deficiencies in citramalate synthase and threonine ammonia-lyase activity. Thus, in *G. sulfurreducens*, 2-oxobutanoate can be synthesized either from citramalate or threonine, with the former being the main pathway for isoleucine biosynthesis. The citramalate synthase of *G. sulfurreducens* constitutes the first characterized member of a phylogenetically distinct clade of citramalate synthases, which contains representatives from a wide variety of microorganisms.

The *Geobacteraceae* are a family of dissimilatory Fe(III) reducing *Deltaproteobacteria* that are predominant members of microbial communities in a diversity of environments where dissimilatory iron reduction is the primary terminal electron accepting process (3, 10, 23, 26, 33, 35, 44). They have been found to play an important role in the natural cycling of Fe(III) and organic compounds, the bioremediation of both organic and metal contamination, and the generation of electricity from organic matter in microbial fuel cells (3, 4, 16, 18, 25, 26, 32). A model of central metabolism was constructed for the genetically tractable *Geobacter* species, *Geobacter sulfurreducens*, based on the results of comparative genomic analyses coupled with physiological and genetic studies (29). This network contained 522 biochemical reactions and 541 unique metabolites, including all 20 amino acids, and was used to create a constraint-based model of *G. sulfurreducens* metabolism which accurately simulated growth via acetate oxidation and the reduction of either Fe(III) citrate or fumarate (29). Many of the amino acid biosynthetic pathways included in the network were analogous to those of *Escherichia coli*, including that for isoleucine (Fig. 1A). In *E. coli*, the first dedicated step in isoleucine biosynthesis is the conversion of threonine to 2-oxobutanoate by the enzyme threonine ammonia-lyase (37). However, alternate precursors for the synthesis of isoleucine have been identified in other organisms, including 2-methylbutyrate, propionate, and citramalate (17, 19, 31, 34, 47). In this study, evidence of two pathways for the biosynthesis of 2-oxobutanoate in *G. sulfurreducens* is presented. Our results indicate that 2-oxobutanoate can be synthesized either from citramalate or threonine, with the former being the main pathway for isoleucine biosynthesis in *G. sulfurreducens*. Homologs of the citramalate synthase of *G. sulfurreducens* (*cimA*) have been found in a wide diversity of microorganisms, particularly, in the *Deltaproteobacteria*.

* Corresponding author. Mailing address: Department of Microbiology, 203N Morrill Science Center IVN, University of Massachusetts Amherst, Amherst, MA 01003. Phone: (413) 577-2439. Fax: (413) 577-4660. E-mail: crisso@microbio.umass.edu.

▽ Published ahead of print on 1 February 2008.

MATERIALS AND METHODS

Bacterial strains and growth conditions. *G. sulfurreducens* (ATCC 51573) (9) strain DL1 was obtained from our laboratory culture collection and used to construct strains DLCR5 (*tdcB*::Kn^r), DLCR6 (*cimA*::Gm^r) and the double mutant DLCR7 (*tdcB*::Kn^r *cimA*::Gm^r) as described below. Strains were cultured under strict anaerobic conditions at 30°C in an atmosphere of N_2 and CO_2 (80%:20%), as previously described (6), in either fresh-water medium (27) or NBAF medium (electron donor, 20 mM acetate; electron acceptor, 40 mM fumarate) (9). Isoleucine was added to a final concentration of 0.02% when required. Antibiotics were added at the following final concentrations: 50 μg/ml for kanamycin and 20 μg/ml for gentamicin.

Nucleic acid manipulations. Genomic DNA preparations and gel extractions were carried out using the Qiagen Genome-tip 100G and Qiaquick Gel Extraction kits, respectively (Qiagen Inc, Valencia, CA).

Construction of mutants via single-step gene replacement. Single-step gene replacement was performed essentially as previously described (9, 24). The sequences of all primers used for the construction and screening of strains DLCR5, DLCR6, and DLCR7 are listed in Table 1. To create a linear DNA fragment for the construction of mutant DLCR5, three primary fragments were generated independently by PCR. The first fragment was amplified from DL1 chromosomal DNA using primers 486-1b and 486-2b (Table 1). The middle segment containing a kanamycin resistance cassette was amplified from plasmid pBBR1MCS-2 (21) with hybrid primers 486-3bKn and 486-4bKn (Table 1). The third fragment was amplified from DL1 chromosomal DNA using primers 486-5b and 486-6b (Table 1). PCR conditions were as follows: 35 cycles of 95°C for 30 s, 58°C for 90 s, and 72°C for 45 s. The reactions were preceded by a 5-min incubation at 95°C during which *Taq* polymerase was added ("hot start") and followed by a 10-min extension period at 72°C. The amplified fragments were gel purified and joined by recombinant PCR. The resulting linear fragment was amplified with distal primers 486-1b and 486-6b (Table 1). PCR conditions during these two steps were as described above except that an extension time of 3 min at 72°C was employed. A similar strategy was used to create a linear DNA

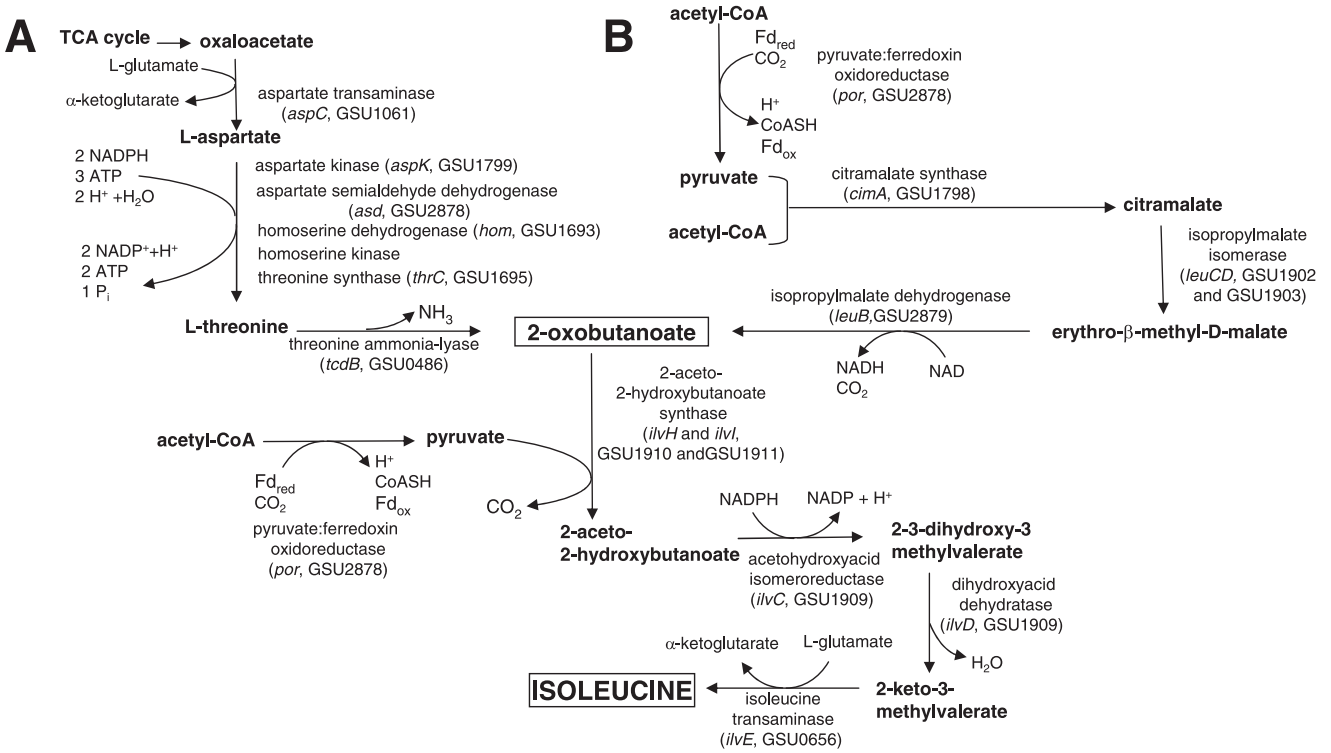

FIG. 1. Pathways for isoleucine biosynthesis in *G. sulfurreducens*. (A) Threonine-dependent pathway (29, 39). (B) Citramalate-dependent pathway, based on that of *L. interrogans* (47).

fragment for the construction of mutant DLCR6 (*cimA*::Gm^r). For this mutant, the first fragment was amplified from DL1 chromosomal DNA using primers 1798-1b and 1798-2b (Table 1). The middle fragment containing a gentamicin resistance cassette was amplified from plasmid pBSL141 (1) with hybrid primers 1798-3Gm2/1798-4Gm2. The third fragment was amplified from DL1 chromosomal DNA with primers 1798-5b and 1798-6b. The individual pieces were joined by recombinant PCR and amplified using the distal primer pairs 1798-1b and 1798-6b. The double mutant DLCR7 was constructed by knocking out the *cimA* gene in DLCR5 using the linear fragment described above.

Electroporation and mutant isolation were carried out as previously described (9, 24) except that the plating medium was supplemented with 0.02% isoleucine. In the case of double mutant DLCR7, the recovered colonies were replica plated onto plates with and without isoleucine, and colonies that failed to grow without 0.02% isoleucine were selected for further analysis. One of each of the mutants was selected as a representative.

In order to confirm the genotypes of the strains, PCRs were carried out with distal primers using chromosomal DNA from DL1 and each of the mutants as template. Distal primers 486-1b and 486-6b span a 1.2-kb fragment in DL1 and a 2.8-kb fragment in DLCR5 (*tdcB*::Kn^r). Similarly, 1798-1b and 1798-6b span a 1-kb fragment in DL1 and a 2.1-kb fragment in DLCR6 (*cimA*::Gm^r) and DLCR7 (*cimA*::Gm^r *tdcB*::Kn^r). In all cases bands of the expected sizes were obtained. The mutant and wild-type strains were also screened with combinations of primers that annealed outside and inside the two mutagenic constructs and thus were expected to yield amplicons only in specific mutants. Primers 486-1b/486-4bKn and 486-3bKn/486-6b were used to confirm the presence of the *tdcB*::Kn^r mutation in strains DLCR5 and DLCR7, while primers 1798-1b/1798-4Gm2 and 1798-3Gm2/1798-6b were used to confirm the presence of the *cimA*::Gm^r mutation in strains DLCR6 and DLCR7. As expected, bands of the correct sizes were obtained from all the mutants but not from the wild type (data not shown).

TABLE 1. Primers used for mutant construction by recombinant PCR

Primer	Coordinate[a]	Length (no. of residues)	Sequence (5′ → 3′)[b]
486-1b	517645	21	CATCACGGGCATTCACACTAG
486-2b	516976	20	CCTTTTGCAGCGAATAGTGG
486-3bKn	Hybrid primer	42	CCACTATTCGCTGCAAAAGGAGCTACTGGGCTATCTGGACAA
486-4bKn	Hybrid primer	41	GATGATGGGAAAGGTGTTCACATCGCTTGGTCGGTCATTTC
486-5b	515892	21	GTGAACACCTTTCCCATCATC
486-6b	515413	19	ATAGCATCGCCGATCTGTG
1798-1b	1965196	20	GGATATTTCCTTCCTCGTGG
1798-2b	1964589	19	GACAATTCCTTCGCTGACC
1798-3Gm2	Hybrid primer	40	GGTCAGCGAAGGAATTGTCACATAAGCCTGTTCGGTTCGT
1798-4Gm2	Hybrid primer	41	GGTGCTCATAGGTTTCAGGAACGGCTTGAACGAATTGTTAG
1798-5b	1964319	20	TCCTGAAACCTATGAGCACC
1798-6b	1963728	20	TCCACACTGTCCAGAAGAGC

[a] Negative strand nucleotide position.
[b] Hybrid primers are composed of *G. sulfurreducens* sequences and antibiotic resistance cassette sequences. The underlined sequences in primers 486-3bKn, 486-4Kn, 1798-3Gm2, and 1798-4Gm2 correspond to the reverse complements of primers 486-2b, 486-5b, 1798-2b, and 1798-5b, respectively.

TABLE 2. Comparison of experimental and predicted mass isotopomer distributions during growth of wild-type *G. sulfurreducens* on acetate-fumarate medium containing 30% [^{13}C]acetate and unlabeled fumarate

Amino acid and mass isotopomer[a]	Experimental mass isotopomer distribution[b]	Predicted MDV[c]		
		Threonine pathway	Citramalate pathway	Both pathways
Aspartate				
M+0	0.9350	0.9572	0.9429	0.9587
M+1	0	0.0339	0.0322	0.0337
M+2	0.0448	0.0080	0.0245	0.0069
M+3	0.0202	0.0009	0.0004	0.0008
Isoleucine				
M+0	0.4428	0.6639	0.3947	0.4477
M+1	0.1246	0.0449	0.1999	0.1348
M+2	0.2829	0.2781	0.2423	0.2730
M+3	0.0891	0.0105	0.1108	0.0901
M+4	0.0425	0.0023	0.0370	0.0388
M+5	0.0180	0.0003	0.0153	0.0156
Leucine				
M+0	0.3711	0.3321	0.3944	0.3458
M+1	0.1673	0.1711	0.2003	0.1769
M+2	0.2851	0.2813	0.2149	0.2736
M+3	0.1213	0.1312	0.1111	0.1271
M+4	0.0555	0.0594	0.0369	0.0539
M+5	0	0.0250	0.0153	0.0227
Total error[d]		0.3608	0.1495	0.0747

[a] The unlabeled molecule is shown as M+0, and numbers above zero correspond to the numbers of additional mass units (^{13}C atoms).
[b] Experimental values are averages of two fragments for each amino acid, both missing the carboxy-terminal carbon atom. The mass isotopomer distributions for these two fragments were the averages of single derivatization reactions performed on extracts prepared from three replicate cultures.
[c] MDVs were calculated by running the optimization routine assuming each pathway separately, and then allowing the optimization routine to select the best-fitting ratio between them.
[d] Errors are the sum of squared differences between predicted and experimental values for aspartate, isoleucine, and leucine fragments.

TABLE 3. Comparison of experimental and predicted mass isotopomer distributions during growth of wild-type *G. sulfurreducens* on acetate-fumarate medium containing unlabeled acetate and 30% [^{13}C]fumarate

Amino acid and mass isotopomer[a]	Experimental mass isotopomer distribution[b]	Predicted MDV[c]		
		Threonine pathway	Citramalate pathway	Both pathways
Aspartate				
M+0	0.7093	0.6908	0.6890	0.6983
M+1	0	0.0256	0.0234	0.0250
M+2	0.2907	0.2836	0.2875	0.2765
M+3	0	0	0.0001	0.0002
Isoleucine				
M+0	0.8662	0.6758	0.8644	0.8619
M+1	0.0263	0.0360	0.0372	0.0393
M+2	0.0967	0.2819	0.0934	0.0952
M+3	0.0087	0.0047	0.0025	0.0020
M+4	0.0020	0.0017	0.0025	0.0016
M+5	0.0001	0	0	0
Leucine				
M+0	0.8937	0.8655	0.8597	0.9196
M+1	0.0409	0.0372	0.0467	0.0407
M+2	0.0415	0.0924	0.0885	0.0383
M+3	0.0052	0.0025	0.0029	0.001
M+4	0.001	0.0025	0.0023	0.0004
M+5	0.0177	0	0	0
Total error[d]		0.3784	0.1271	0.0622

[a] The unlabeled molecule is shown as M+0, and numbers above zero correspond to the number of additional mass units (^{13}C atoms).
[b] Experimental values are averages of two fragments for each amino acid, both missing the carboxy-terminal carbon atom. The mass isotopomer distributions for these two fragments were the averages of three derivatizations performed on extracts prepared from pooled duplicate cultures.
[c] MDVs were calculated by running the optimization routine assuming each pathway separately, and then allowing the optimization routine to select the best-fitting ratio between them.
[d] Errors are the sum of squared differences between predicted and experimental values for aspartate, isoleucine, and leucine fragments.

Analytical techniques. Growth of fumarate cultures was assessed by measuring optical density at 600 nm with a Genesys 2 spectrophotometer (Spectronic Instruments, Rochester, NY). The organic acid content of the culture medium was determined by high-pressure liquid chromatography using an LC-10AT high-pressure liquid chromatograph (Shimadzu, Kyoto, Japan) equipped with an Aminex HPX-87H column (300 by 7.8 mm; Bio-Rad, Hercules, CA). Organic acids were eluted in 8 mM H_2SO_4 and quantitated with an SPD-10VP UV detector (Shimadzu, Kyoto, Japan) set at 215 nm. Fe(II) concentrations were determined with a ferrozine assay as previously described (28). Protein concentrations were determined by the bicinchoninic acid method with bovine serum albumin as a standard (40).

^{13}C labeling. For the ^{13}C labeling experiments described in Tables 2 and 3, cells were grown in fresh-water medium containing either 10 mM acetate (30% [$^{13}C_2$]acetate–70% unlabeled acetate [mol/mol]) and 27.5 mM unlabeled fumarate or 10 mM unlabeled acetate and 27.5 mM fumarate (30% [2,3-$^{13}C_2$]fumarate–70% unlabeled fumarate [mol/mol]). (The labeled compounds are abbreviated hereafter as [^{13}C]acetate and [^{13}C]fumarate, respectively.) Note that "unlabeled" in this context means containing the natural abundance of 1.07% ^{13}C in each carbon atom. For the ^{13}C labeling experiments performed to compare the wild-type and the mutant strains, cells were grown in NBAF medium containing 20 mM acetate (30% [^{13}C]acetate–70% unlabeled acetate [mol/mol]) and 40 mM unlabeled fumarate. ^{13}C compounds were purchased from Sigma-Aldrich Corporation (St. Louis, MO).

Processing and GC-mass spectrometry analysis of ^{13}C-labeled samples. Cells were cultured for a minimum of two 5% transfers in ^{13}C-labeled medium prior to harvesting at mid-log phase by centrifugation at 3,000 × *g*. Cell pellets were resuspended in isotonic buffer, pH 7 (4.19 g/liter morpholinepropanesulfonic acid, 0.6 g/liter $NaH_2PO_4 \cdot H_2O$, 0.1 g/liter KCl, 5 g/liter NaCl, 10 ml of Mg-Ca mix [pH 7]; Mg-Ca mix contains 3 g/liter $MgSO_4 \cdot 7H_2O$ and 0.1 g/liter $CaCl_2 \cdot 2H_2O$), pelleted for 15 min at 3,000 × *g*, and resuspended in 4 ml of ice-cold 50 mM potassium phosphate buffer, pH 7.5. Cells were then disrupted by sonication and cleared by ultracentrifugation (1 h at 25,700 × *g* at 4°C). For each derivatization, 200 μg of total protein was hydrolyzed in 6 M HCl for 24 h at 105°C, extracted with chloroform to remove residual lipids, and evaporated at 65°C. The pellet was resuspended in 100 μl of tetrahydrofuran, and the amino acids were derivatized by adding 100 μl of *N*-(tert-butyldimethylsilyl)-*N*-methyltrifluroacetamide (Sigma Aldrich) (2, 12) and incubating for 60 min at 75°C. Derivatized amino acids were analyzed using a Hewlett-Packard HP G1723A gas chromatograph (GC)-quadrupole mass selective detector (electron impact), equipped with a DB-5 column (Agilent Technologies). The GC oven was held at 150°C for 2 min, ramped to 240°C at 3°C per min, ramped at 20°C per min to 300°C, and then held for 5 min. The helium flow rate was 0.7 ml/min, the source temperature was 200°C, the interface temperature was 250°C, and the quadrupole temperature was 105°C. A solvent delay of 3 min was used. Each derivatized sample was injected three times. Amino acids were identified based on known fragmentation patterns and associated masses (11). Raw mass isotopomer data were corrected for naturally occurring ^{13}C in the derivatization reagents and noncarbon isotopes in the entire fragment using a well-established spreadsheet method (12, 43).

Development of the isotopomer balance model. A reduced metabolic model of *G. sulfurreducens*, containing 209 reactions and 143 metabolites, was derived from the genome-scale model (29) by retaining only those reactions involved in central carbon and amino acid metabolism. The reduced network contained 79 reversible reactions, which added an additional level of complexity, since both

forward and reverse reaction rates affect the observed isotopomer distribution. This is typically addressed by using net fluxes and exchange coefficients (11, 45). The 79 exchange coefficients for the reversible reactions, therefore, constituted additional adjustable parameters which had to be determined using the isotopomer model. Finally, redox and ATP balances were incorporated into the flux analysis model as constraints in order to make the calculated optimum feasible. For simplicity, NADH and NADPH were considered equivalent, and the electron transport chain was represented by a single reaction. Isotopomer mapping matrices (IMMs) describe the transfer of carbon atoms from the reactants to products and are a property of a given reaction independent of the particular model (38). IMMs for the majority of the reactions were obtained from an *E. coli* isotopomer model of similar size (41). The IMMs for the remaining *Geobacter*-specific reactions were created by hand, based on known biochemistry.

Calculation of bounds on exchange fluxes. In order to establish bounds on the exchange fluxes, the rates of acetate and fumarate uptake as well as succinate and biomass production were determined by periodically sampling the cultures. Effective fumarate uptake was determined by two measurements: (i) fumarate depletion minus malate accumulation or (ii) succinate accumulation. In order to maintain consistency among experiments, all rates were then normalized to a flux of 10 mmol g (dry weight)$^{-1}$ h^{-1} acetate uptake. Because of variability in the measurements, constraints were set as ranges rather than fixed values, with the ranges determined by error propagation of the standard deviations of the measurements. The values calculated for fumarate uptake were very consistent, and for each case the wider range of the two calculated was used.

Flux analysis calculations. The isotopomer balance algorithm calculated the predicted set of isotopomer distribution vectors (IDVs) for all metabolites in the network for a given flux distribution. The input was a random flux distribution and set of exchange coefficients that were within specified bounds and satisfied the overall metabolite balance, $S \cdot v = 0$, where S is the stoichiometric matrix for the reaction network and v is the vector of net reaction fluxes. Through each iteration, the IDV of compound i was calculated as follows:

$$\mathrm{IDV}_i = \frac{1}{\sum_{k=1}^{M} v^k_{i,\mathrm{out}}} \times \sum_{k=1}^{M}\left[v^k_{i,\mathrm{in}} \prod_{j=1}^{n_k} (\mathrm{IMM}^k_{j\rightarrow i} \times \mathrm{IDV}_j)\right]$$

where M is the total number of reactions in the network, n_k is the number of substrates in reaction k, $v^k_{i,\mathrm{out}}$ is the flux of metabolite i in reaction k if it is consumed, and $v^k_{i,\mathrm{in}}$ is the flux if it is produced. The resulting program was model independent. It generated the isotopomer balance once the stoichiometric matrix and list of IMMs were supplied and calculated all IDVs given the input flux distribution and isotopomer distribution of the feed molecules acetate and fumarate (41). Subsequently, these IDVs were converted to mass distribution vectors (MDVs), column vectors containing mole fractions for groups of isotopomers with the same mass for all observable products (46). The genetic strategy that creates diversity in a "population" of flux distributions through small changes in the parameter values (mutation) or combination of parameters from two different "parent" flux distributions (7, 15) was used as the optimization routine for flux analysis. An initial population size of 1,000 was used, and optimizations were run until the routine converged on a minimum, usually within 100 generations. The objective value was the sum-of-squares difference between the measured and calculated MDV values, weighted by the standard deviations in order to favor the most accurate measurements. Only aspartate, leucine, and isoleucine (two fragments each) were included in the optimization. Use of this reduced data set increased the computational speed, reduced the number of local minima, and allowed us to focus specifically on the isoleucine problem. Since there was no guarantee that this minimum was global, the routine was repeated several times for each experiment, and the lowest error result was selected as the true measured flux distribution. The isotopomer balance and optimization routines were coded in Matlab (The Mathworks, Natick, MA).

Enzymatic assays. For the initial biochemical characterization of the wild-type strain, cells were cultured in fresh-water medium containing 10 mM acetate and 27.5 mM fumarate and harvested at mid-log phase. For biochemical assays comparing the wild-type and mutant strains, cells were grown in NBAF medium and harvested at early stationary phase. Soluble extracts were prepared as described above, aliquoted, and stored at −80°C. Threonine and serine ammonia-lyase activities were assayed essentially as previously described (22) by measuring the production of ketone (either 2-oxobutanoate or pyruvate) colorimetrically with 2,4-dinitrophenyl hydrazine, except that NH_4Cl was omitted, and the final concentration of threonine was 50 mM. The citramalate synthase activity was assessed by monitoring the pyruvate-dependent release of coenzyme A (CoA) from acetyl-CoA as previously described (17) with the following modifications: the samples were incubated at 37°C, the concentration of acetyl-CoA was 0.5 mM, and 0.1% sodium dodecyl sulfate was added to the stop solution. The assay for isopropylmalate synthase was identical to the citramalate synthase assay, except that pyruvate was replaced with α-ketoisovalerate.

RESULTS AND DISCUSSION

Evidence for an alternate isoleucine biosynthesis pathway in *G. sulfurreducens*. ^{13}C metabolic flux analysis can be used as a tool for verifying genome annotation, optimizing metabolic models, and elucidating the physiological state of microorganisms (11). In order to test the accuracy of the reconstructed central metabolic network of *G. sulfurreducens*, ^{13}C labeling studies were initiated. An isotopomer balance model for *G. sulfurreducens*, with the IMMs taken largely from an *E. coli* model (41), was developed.

In these studies, *G. sulfurreducens* was cultured in fresh-water acetate-fumarate medium containing either 30% (mol/mol) [^{13}C]acetate (labeled at both carbons) or ^{13}C]fumarate (labeled at carbons 2 and 3). During growth on this medium, the tricarboxylic acid cycle (TCA) cycle functions as an open loop in which the succinate dehydrogenase reaction is bypassed (13). Continual flux through the remaining reactions of the TCA cycle is maintained by coupling the secretion of succinate to the uptake of fumarate via the dicarboxylate exchanger, DcuB (5, 13, 29, 42). As a result, the TCA cycle intermediate, oxaloacetate, is derived primarily from exogenous fumarate. In fact, during growth on acetate-[^{13}C]fumarate medium, the mass isotopomer distribution of aspartate, which derives from oxaloacetate, matched that of the feed (30% doubly labeled/70% unlabeled). In contrast, during growth on [^{13}C]acetate-fumarate medium, aspartate was primarily unlabeled (Tables 2 and 3), confirming the presence of the open loop. Pyruvate is another common amino acid precursor. In *G. sulfurreducens*, pyruvate biosynthesis occurs primarily via the condensation of acetyl-CoA and CO_2 by the pyruvate-ferredoxin oxidoreductase (39). In fact, leucine, which was predicted to be derived from acetyl-CoA and pyruvate, was labeled during growth on [^{13}C]acetate-fumarate, and essentially unlabeled during growth on acetate-[^{13}C]fumarate, confirming the central role of the pyruvate-ferredoxin oxidoreductase in pyruvate biosynthesis.

According to the annotated pathway (Fig. 1A), both oxaloacetate and pyruvate serve as precursors for isoleucine biosynthesis, and thus this amino acid should be labeled in the presence of both [^{13}C]acetate and [^{13}C]fumarate (Tables 2 and 3, threonine-dependent pathway). However, the isotopomer mass distribution of isoleucine did not match the expected pattern: isoleucine was extensively labeled in the presence of [^{13}C]acetate but poorly labeled in the presence of [^{13}C]fumarate (Tables 2 and 3). This suggested that the annotated threonine-dependent pathway did not play a major role in isoleucine biosynthesis and that acetyl-CoA and/or pyruvate was the predominant precursor for this amino acid.

In the spirochete *Leptospira interrogans* and in methanogenic *Archaea*, the key isoleucine precursor, 2-oxobutanoate, is synthesized from acetyl-CoA and pyruvate via the citramalate pathway (17, 34, 47) (Fig. 1B). The first dedicated step in this pathway is the condensation of pyruvate and acetyl-CoA by the enzyme citramalate synthase (CimA; EC 4.1.3.22). The introduction of this pathway into the *G. sulfurreducens* isotopomer

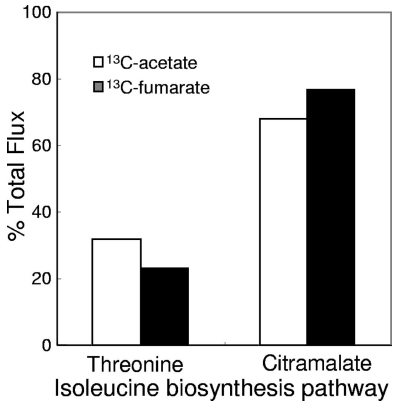

FIG. 2. Predicted contributions of the threonine and citramalate pathways to isoleucine biosynthesis in wild-type *G. sulfurreducens* cultured in acetate-fumarate medium containing either 30% (mol/mol) [^{13}C]acetate or [^{13}C]fumarate. Model predictions are the best fit flux distributions, assuming both pathways are active.

balance model significantly improved the agreement of experimental and predicted isotopomer mass distributions (Tables 2 and 3). The best fit was generated by allowing flux through both pathways, with the citramalate pathway serving as the primary route of isoleucine biosynthesis (Fig. 2), accounting for 68 to 77% of the total flux to isoleucine.

In order to determine whether the citramalate pathway was active in *G. sulfurreducens*, crude soluble extracts were prepared from mid-log, freshwater acetate-fumarate cultures grown under the same conditions as those used for ^{13}C flux analysis studies and tested for the presence of citramalate synthase activity. These extracts contained 5.94 ± 0.49 nmol mg^{-1} min^{-1} of citramalate synthase activity, measured as the pyruvate-dependent release of CoA from acetyl-CoA (47). The citramalate synthase appeared to have a high affinity for pyruvate, with 52.5% ± 4.9% of the activity remaining when the pyruvate concentration was reduced from 1 mM to 0.1 mM. Although these results were consistent with the presence of citramalate synthase, they were not conclusive due to the fact that isopropylmalate synthase, which catalyzes the first step in leucine biosynthesis, has residual citramalate synthase activity (20, 34, 47). In addition, high levels of pyruvate-independent CoA release interfered with detection of the enzyme activity and accurate determination of the K_m for pyruvate.

Because both ^{13}C labeling studies and preliminary biochemical studies were consistent with the presence of citramalate synthase in *G. sulfurreducens*, we examined the genome for candidate genes. Only two citramalate synthases had been characterized, those of *L. interrogans* and *Methanocaldococcus jannaschii* (17, 47). Both citramalate synthases were homologous to isopropylmalate synthase (LeuA), which catalyzes the first step in the biosynthesis of leucine (47). Examination of the

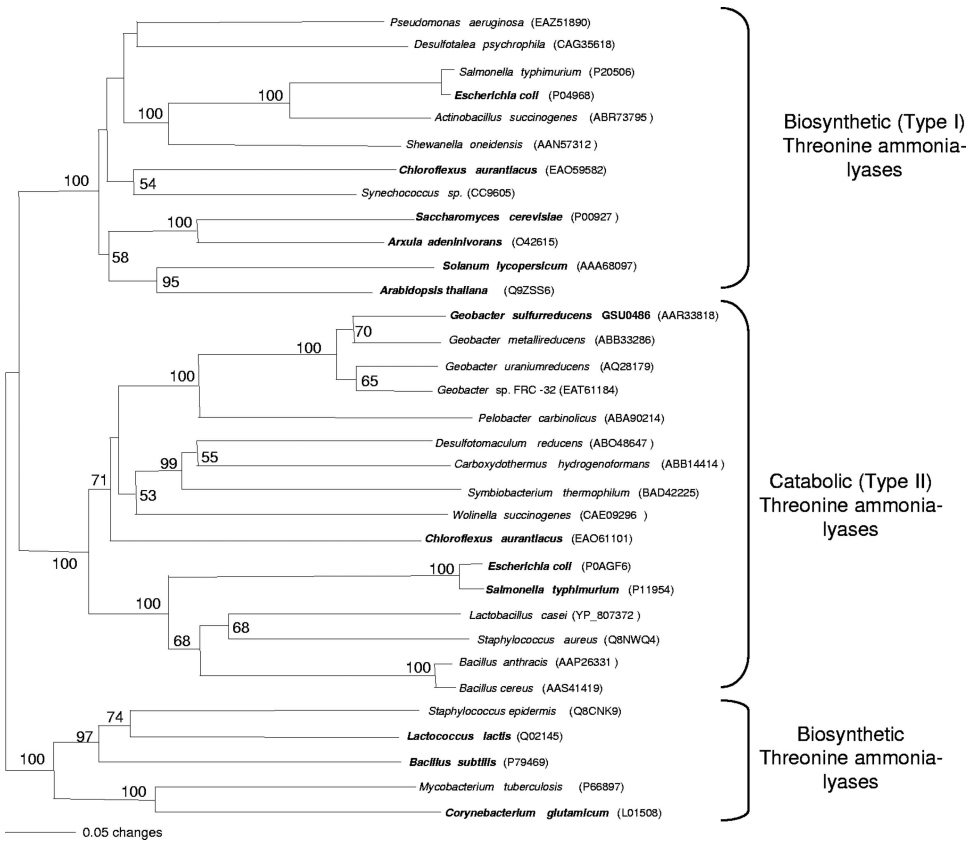

FIG. 3. Phylogenetic analysis of threonine ammonia-lyases. The phylogenetic tree was inferred from protein sequences by the neighbor-joining method using the BIONJ algorithm (14, 36) as previously described (8). Bootstrap values were calculated for 100 replicates. Biochemically or genetically characterized ammonia-lyases are indicated in bold type.

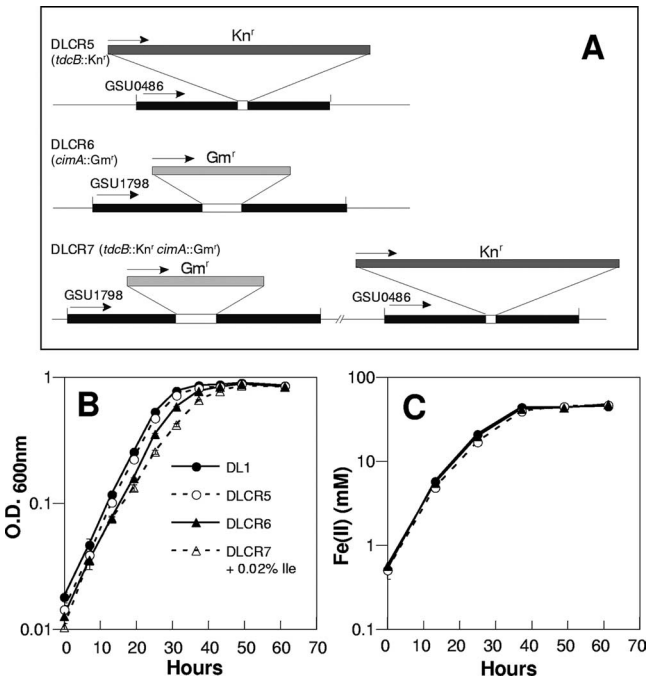

FIG. 4. Construction and phenotypic characterization of citramalate synthase and threonine ammonia-lyase knockout mutants. (A) Scaled representation of the genotypes of mutants DLCR5, DLCR6, and DLCR7. White sections represent the deleted section of each gene. Arrows indicate orientation of genes and antibiotic resistance cassettes. Growth of wild-type (DL1) and mutant strains in acetate-fumarate medium (NBAF) (B) and in fresh-water medium with 20 mM acetate and 56 mM ferric citrate (C). Inocula (3%) were log-phase acetate-fumarate cultures. Each determination represents the average and standard deviation of triplicate cultures. OD, optical density.

G. sulfurreducens genome revealed three LeuA family members: GSU1906, GSU1798, and GSU0937. Comparison to characterized enzymes suggested that GSU1906, which has 65% sequence similarity to LeuA of *Salmonella enterica* serovar Typhimurium, encoded an isopropylmalate synthase, whereas GSU0937, which has 65% sequence similarity to NifV of *Azotobacter vinelandii*, encoded a homocitrate synthase. The remaining candidate, GSU1798, which was annotated as a LeuA homolog (30), is equally similar to characterized isopropylmalate and citramalate synthases; it is 46% similar to *S. enterica* serovar Typhimurium LeuA and 45% similar to CimA from both *L. interrogans* and *M. jannaschii*. Thus, it was selected as the most likely candidate for a citramalate synthase in *G. sulfurreducens*.

Because flux analysis indicated that the threonine-dependent pathway was a relatively minor contributor to isoleucine biosynthesis, we reexamined the genomic evidence for this pathway. Threonine ammonia-lyase (GSU0486) was the only enzyme unique to this pathway. Phylogenetic analysis of GSU0486, which was annotated as a biosynthetic threonine ammonia-lyase, IlvA (30), revealed that it clustered with catabolic threonine ammonia-lyases (TdcB; EC 4.3.1.19), which are not inhibited by isoleucine and also catalyze the deamination of serine (37) (Fig. 3). Soluble extracts prepared from *G. sulfurreducens* grown under the same conditions as the initial flux analysis experiment (log-phase, fresh-water acetate-fumarate medium) contained 227.9 ± 6.2 nmol mg^{-1} min^{-1} of isoleucine-insensitive threonine ammonia-lyase and 31.7 ± 2.3 nmol mg^{-1} min^{-1} of serine ammonia-lyase activity.

TABLE 4. Enzymatic activities in wild-type and mutant strains

Strain (description)	Activity of the indicated enzyme (nmol mg of protein^{-1} min^{-1})[a]			
	Thr ammonia-lyase	Ser ammonia-lyase	Citramalate synthase	Isopropyl malate synthase
DL1 (wild type)	189 ± 46	41 ± 6.2	7.4 ± 0.2	8.3 ± 0.4
DLCR5 (*tdcB*::Kn^r)	ND	ND	5.1 ± 0.2	8.5 ± 0.7
DLCR6 (*cimA*::Gm^r)	217 ± 24	–	0.4 ± 0.3	9.2 ± 0.3
DLCR7 (*tdcB*::Kn^r *cimA*::Gm^r)	ND	–	0.4 ± 0.4	18.1 ± 1.3

[a] Measurements are averages and standard deviations of triplicate assays. Soluble extracts were prepared from early-stationary-phase NBAF cultures. ND, not detected; –, not assayed.

TABLE 5. Comparison of experimental and predicted mass isotopomer distributions during growth of wild-type (DL1) and mutant (DLCR5 and DLCR6) strains on acetate-fumarate medium containing 30% [^{13}C]acetate and unlabeled fumarate

Strain (description) and isoleucine mass isotopomer[a]	Experimental mass isotopomer distributions[b]	Predicted MDV[c]
DL1 (wild type)		
M+0	0.4259	0.4116
M+1	0.1316	0.1575
M+2	0.2912	0.2667
M+3	0.0893	0.1043
M+4	0.0465	0.0424
M+5	0.0155	0.0175
Total error		0.0858
DLCR5 (*tdcB*::Kn^r)		
M+0	0.3795	0.3735
M+1	0.1536	0.1735
M+2	0.2824	0.2683
M+3	0.1091	0.1170
M+4	0.0526	0.0480
M+5	0.0228	0.0197
Total error		0.0700
DLCR6 (*cimA*::Gm^r)		
M+0	0.6683	0.6595
M+1	0.0417	0.0579
M+2	0.2653	0.2516
M+3	0.0142	0.0191
M+4	0.0081	0.0101
M+5	0.0024	0.0018
Total error		0.0705

[a] The unlabeled molecule is shown as M+0, and numbers above zero correspond to the numbers of additional mass units (^{13}C atoms). Errors are the sum of squared differences between predicted and experimental values for isoleucine fragments.

[b] Experimental values are averages of two isoleucine fragments, both missing the carboxy-terminal carbon atom.

[c] MDVs were calculated by allowing the optimization routine to select the best-fitting ratio between the threonine and citramalate pathways.

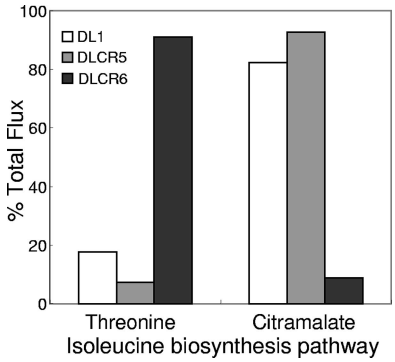

FIG. 5. Predicted contributions of threonine and citramalate pathways to isoleucine biosynthesis in the wild-type (DL1) and mutant strains during growth on acetate-fumarate (NBAF) medium. Model predictions are the best fit flux distributions, assuming both pathways are active.

Genetic evidence for two isoleucine biosynthetic pathways. In order to corroborate the results of the preliminary biochemical analysis and evaluate the functions of the putative threonine ammonia-lyase (GSU0486; *tdcB*) and citramalate synthase (GSU1798; *cimA*) genes, three mutant strains were constructed: a threonine ammonia-lyase knockout mutant (DLCR5; *tdcB*::Kn^r), a citramalate synthase knockout mutant (DLCR6; *cimA*::Gm^r), and a double knockout mutant (DLCR7; *tdcB*::Kn^r *cimA*::Gm^r) (Fig. 4A). The single mutants grew on the standard plating medium, whereas the double mutant grew only on plates supplemented with 0.02% isoleucine. This indicated that there were no other pathways generating the key precursor 2-oxobutanoate and that both pathways contributed to the biosynthesis of isoleucine. Moreover, these genes could compensate for each other. During growth on acetate-fumarate medium (Fig. 4B), the growth rate and biomass yields of both single mutants were very similar to wild type, albeit there was a small increase in the doubling time of the citramalate synthase-deficient mutant relative to wild type (6 ± 0.13 h versus 5.25 ± 0.18 h). During growth on acetate-Fe(III) citrate medium, the rate of Fe(III) citrate reduction (Fig. 4C) and the final biomass yields of the two single mutants (data not shown) were essentially identical to the wild type.

In order to confirm that GSU0486 and GSU1798 coded for threonine ammonia-lyase and citramalate synthase, respectively, soluble extracts of the wild-type and the three mutant strains were prepared from early-stationary-phase NBAF cultures, and enzymatic assays were performed (Table 4). In the wild-type strain, the two activities were comparable to those obtained from extracts prepared from mid-log fresh-water medium cultures. As expected, threonine ammonia-lyase and

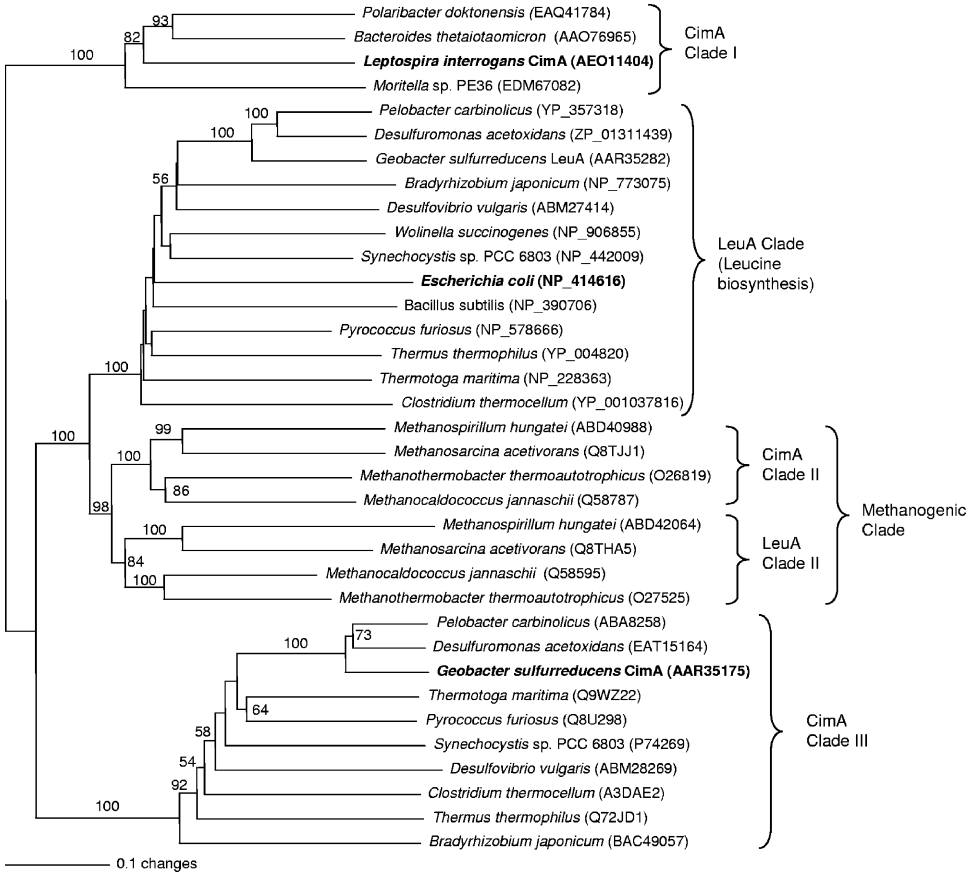

FIG. 6. Phylogenetic analysis of citramalate synthases. Phylogenetic tree was inferred from protein sequences by the neighbor-joining method using the BIONJ algorithm (14, 36) as previously described (8). Bootstrap values were calculated for 100 replicates. Biochemically or genetically characterized citramalate synthases are indicated in bold type.

serine ammonia-lyase activities were undetectable in DLCR5. Likewise, citramalate synthase activity was greatly reduced in DLCR6. Neither activity could be detected in the isoleucine auxotroph DLCR7. Isopropylmalate synthase activity was assayed as an internal control and was found to be identical or higher than wild type in the three mutant strains. These results indicate that the current annotation of GSU0486 as *ilvA* and GSU1798 as a *leuA* homolog does not reflect their actual enzymatic activities. We propose that they be reannotated as threonine/serine ammonia-lyase (*tdcB*) and citramalate synthase (*cimA*), respectively.

Unlike the closely related catabolic ammonia lyases of *E. coli* and *S. enterica* serovar Typhimurium, which have a strictly biodegradative role in these organisms (37), the threonine ammonia-lyase of *G. sulfurreducens* clearly participates in isoleucine biosynthesis. Despite the fact that the contribution of the threonine-dependent pathway to isoleucine biosynthesis in the wild-type strain was relatively minor (18 to 30%) (Fig. 2), the amount of threonine ammonia-lyase activity in soluble extracts was about 25-fold higher than that of citramalate synthase activity. This discrepancy could be due to low intracellular concentrations of threonine and/or to inhibition of the enzyme by pyruvate, which occurs in *E. coli* (37). A detailed biochemical characterization of these enzymes coupled with measurements of intracellular concentrations of amino acids and metabolites is therefore warranted.

In order to corroborate the roles of the citramalate synthase and the threonine ammonia-lyase in isoleucine biosynthesis, ^{13}C labeling studies were conducted in all three mutants and the wild-type strain. Isoleucine was 90 to 95% unlabeled in the isoleucine auxotroph DLCR7 (data not shown). A clear shift in the isoleucine flux ratio to primary use of the citramalate-dependent pathway in DLCR5 and the threonine-dependent pathway in DLCR6 was observed (Table 5 and Fig. 5). The residual fluxes in the deleted pathway in each case were likely due to imperfect model fit to the experimental data. Error in flux ratios can result from random variations in mass spectrometry data, loss of information in converting positional isotopomer distributions to mass isotopomer distributions of measurable fragments, and the nonlinearity of the optimization problem (45).

Distribution of the citramalate synthase. The CimA protein from *G. sulfurreducens* constitutes the first characterized member of a phylogenetically distinct clade of citramalate synthases (Fig. 6, clade III). This clade contains representatives from a wide range of bacteria including *Deltaproteobacteria*, *Alphaproteobacteria*, *Cyanobacteria*, *Deinococci*, and *Clostridia* as well as members of the *Archaea*, such as *Thermococcaceae*. Clade III representatives were also found in the *Actinobacteria*, *Sphingobacteria*, *Chlorobia*, and the *Chloroflexi*. Inclusion of the LeuA and CimA sequences from these organisms did not affect the structure of the phylogenetic tree (data not shown). Clade III CimA homologs appear to be absent from the *Beta-*, *Epsilon-*, and *Gammaproteobacteria*. In some organisms that lack homologs of threonine ammonia-lyase, this class of citramalate synthases may constitute the only route for isoleucine biosynthesis; examples include *Pelobacter propionicus*, *Pyrococcus furiosus*, and all sequenced members of the *Desulfovibrionaceae*.

Implications. There are two pathways involved in isoleucine biosynthesis in *G. sulfurreducens*: the threonine-dependent pathway and the citramalate-dependent pathway (Fig. 1). Our results indicate that the citramalate-dependent pathway is the major route for isoleucine biosynthesis in *G. sulfurreducens*. This conclusion is supported by genetic, biochemical, and ^{13}C-labeling data. The citramalate synthase of *G. sulfurreducens* represents a novel phylogenetic variant of the enzyme. Furthermore, the wide distribution of this novel class of citramalate synthases throughout the microbial world indicates that the citramalate-dependent pathway of isoleucine biosynthesis is fairly common.

ACKNOWLEDGMENTS

This research was supported by the Office of Science (BER), U.S. Department of Energy, grants DE-GC02-02ER 63446 and DE-FG02-01ER63221.

We thank members of Steven Petsch's laboratory, especially Mike Formolo and Elizabeth Gordon, for their assistance with the GC-MS analysis. We also thank Laura Valinotto for her excellent technical assistance.

REFERENCES

1. **Alexeyev, M. F., I. N. Shokolenko, and T. P. Croughan.** 1995. Improved antibiotic-resistance gene cassettes and omega elements for *Escherichia coli* vector construction and in vitro deletion/insertion mutagenesis. Gene **160:** 63–67.
2. **Al Zaid Siddiquee, K., M. Arauzo-Bravo, and K. Shimizu.** 2004. Metabolic flux analysis of *pykF* gene knockout *Escherichia coli* based on ^{13}C-labeling experiments together with measurements of enzyme activities and intracellular metabolite concentrations. Appl. Microbiol. Biotechnol. **63:**407–417.
3. **Anderson, R., J. N. Rooney-Varga, C. V. Gaw, and D. R. Lovley.** 1998. Anaerobic benzene oxidation in the Fe(III) reduction zone of petroleum-contaminated aquifers. Environ. Sci. Technol. **32:**1222–1229.
4. **Bond, D. R., D. E. Holmes, L. M. Tender, and D. R. Lovley.** 2002. Electrode-reducing microorganisms that harvest energy from marine sediments. Science **295:**483–485.
5. **Butler, J. E., R. H. Glaven, A. Esteve-Nunez, C. Nunez, E. S. Shelobolina, D. R. Bond, and D. R. Lovley.** 2006. Genetic characterization of a single bifunctional enzyme for fumarate reduction and succinate oxidation in *Geobacter sulfurreducens* and engineering of fumarate reduction in *Geobacter metallireducens*. J. Bacteriol. **188:**450–455.
6. **Caccavo, F. J., D. J. Lonergan, D. R. Lovley, M. Davis, J. F. Stolz, and M. J. McInerney.** 1994. *Geobacter sulfurreducens* sp. nov., a hydrogen- and acetate-oxidizing dissimilatory metal-reducing microorganism. Appl. Environ. Microbiol. **60:**3752–3759.
7. **Christensen, B., and J. Nielsen.** 2000. Metabolic network analysis of *Penicillium chrysogenum* using ^{13}C-labeled glucose. Biotechnol. Bioeng. **68:** 652–659.
8. **Coppi, M. V.** 2005. The hydrogenases of *Geobacter sulfurreducens*: a comparative genomic perspective. Microbiology **151:**1239–1254.
9. **Coppi, M. V., C. Leang, S. J. Sandler, and D. R. Lovley.** 2001. Development of a genetic system for *Geobacter sulfurreducens*. Appl. Environ. Microbiol. **67:**3180–3187.
10. **Cummings, D. E., O. L. Snoeyenbos-West, D. T. Newby, A. M. Niggemyer, D. R. Lovley, L. A. Achenbach, and R. F. Rosenzweig.** 2003. Diversity of *Geobacteraceae* species inhabiting metal-polluted freshwater lake sediments ascertained by 16S rDNA analyses. Microb. Ecol. **46:**257–269.
11. **Dauner, M., and U. Sauer.** 2000. GC-MS analysis of amino acids rapidly provides rich information for isotopomer balancing. Biotechnol. Prog. **16:** 642–649.
12. **Fischer, E., and U. Sauer.** 2003. Metabolic flux profiling of *Escherichia coli* mutants in central carbon metabolism using GC-MS. Eur. J. Biochem. **270:** 880–891.
13. **Galushko, A. S., and B. Schink.** 2000. Oxidation of acetate through reactions of the citric acid cycle by *Geobacter sulfurreducens* in pure culture and in syntrophic coculture. Arch. Microbiol. **174:**314–321.
14. **Gascuel, O.** 1997. BIONJ: an improved version of the NJ algorithm based on a simple model of sequence data. Mol. Biol. Evol. **14:**685–695.
15. **Gombert, A. K., M. M. dos Santos, B. Christensen, and J. Nielsen.** 2001. Network identification and flux quantification in the central metabolism of *Saccharomyces cerevisiae* under different conditions of glucose repression. J. Bacteriol. **183:**1441–1451.
16. **Holmes, D. E., D. R. Bond, R. A. O'Neil, C. E. Reimers, and D. R. Lovley.** 2004. Microbial communities associated with electrodes harvesting electricity from a variety of aquatic sediments. Microb. Ecol. **48:**178–190.
17. **Howell, D. M., H. Xu, and R. H. White.** 1999. (*R*)-Citramalate synthase in methanogenic archaea. J. Bacteriol. **181:**331–333.

18. **Istok, J., J. Senko, L. Krumholz, D. Watson, M. Bogle, A. Peacock, Y. Chang, and D. White.** 2004. In situ bioreduction of technetium and uranium in a nitrate-contaminated aquifer. Environ. Sci. Technol. **38:**468–475.
19. **Kisumi, M., S. Komatsubara, and I. Chibata.** 1977. Pathway for isoleucine formation from pyruvate by leucine biosynthetic enzymes in leucine-accumulating isoleucine revertants of *Serratia marcescens*. J. Biochem. (Tokyo) **82:**95–103.
20. **Kohlhaw, G., T. R. Leary, and H. E. Umbarger.** 1969. Alpha-isopropylmalate synthase from *Salmonella typhimurium*. Purification and properties. J. Biol. Chem. **244:**2218–2225.
21. **Kovach, M. E., P. H. Elzer, D. S. Hill, G. T. Robertson, M. A. Farris, R. M. Roop II, and K. M. Peterson.** 1995. Four new derivatives of the broad-host-range cloning vector pBBR1MCS, carrying different antibiotic-resistance cassettes. Gene **166:**175–176.
22. **Lawther, R. P., and G. W. Hatfield.** 1978. A site of action for tRNA mediated regulation of the *ilvOEDA* operon of *Escherichia coli* K12. Mol. Gen. Genet. **167:**227–234.
23. **Lin, B., M. Braster, B. M. van Breukelen, H. W. van Verseveld, H. V. Westerhoff, and W. F. Roling.** 2005. *Geobacteraceae* community composition is related to hydrochemistry and biodegradation in an iron-reducing aquifer polluted by a neighboring landfill. Appl. Environ. Microbiol. **71:**5983–5991.
24. **Lloyd, J. R., C. Leang, A. L. Hodges Myerson, M. V. Coppi, S. Cuifo, B. Methe, S. J. Sandler, and D. R. Lovley.** 2003. Biochemical and genetic characterization of PpcA, a periplasmic c-type cytochrome in *Geobacter sulfurreducens*. Biochem. J. **369:**153–161.
25. **Lovley, D. R.** 2006. Bug juice: harvesting electricity with microorganisms. Nat. Rev. Microbiol. **4:**497–508.
26. **Lovley, D. R., D. E. Holmes, and K. P. Nevin.** 2004. Dissimilatory Fe(III) and Mn(IV) reduction. Adv. Microb. Physiol. **49:**219–286.
27. **Lovley, D. R., and E. J. P. Phillips.** 1988. Novel mode of microbial energy metabolism: organic carbon oxidation coupled to dissimilatory reduction of iron or manganese. Appl. Environ. Microbiol. **54:**1472–1480.
28. **Lovley, D. R., and E. J. P. Phillips.** 1986. Organic matter mineralization with the reduction of ferric iron in anaerobic sediments. Appl. Environ. Microbiol. **51:**683–689.
29. **Mahadevan, R., D. R. Bond, J. E. Butler, A. Esteve-Nunez, M. V. Coppi, B. O. Palsson, C. H. Schilling, and D. R. Lovley.** 2006. Characterization of metabolism in the Fe(III)-reducing organism *Geobacter sulfurreducens* by constraint-based modeling. Appl. Environ. Microbiol. **72:**1558–1568.
30. **Methe, B. A., K. E. Nelson, J. A. Eisen, I. T. Paulsen, W. Nelson, J. F. Heidelberg, D. Wu, M. Wu, N. Ward, M. J. Beanan, R. J. Dodson, R. Madupu, L. M. Brinkac, S. C. Daugherty, R. T. DeBoy, A. S. Durkin, M. Gwinn, J. F. Kolonay, S. A. Sullivan, D. H. Haft, J. Selengut, T. M. Davidsen, N. Zafar, O. White, B. Tran, C. Romero, H. A. Forberger, J. Weidman, H. Khouri, T. V. Feldblyum, T. R. Utterback, S. E. Van Aken, D. R. Lovley, and C. M. Fraser.** 2003. Genome of *Geobacter sulfurreducens*: metal reduction in subsurface environments. Science **302:**1967–1969.
31. **Monticello, D. J., R. S. Hadioetomo, and R. N. Costilow.** 1984. Isoleucine synthesis by *Clostridium sporogenes* from propionate or alpha-methylbutyrate. J. Gen. Microbiol. **130:**309–318.
32. **North, N. N., S. L. Dollhopf, L. Petrie, J. D. Istok, D. L. Balkwill, and J. E. Kostka.** 2004. Change in bacterial community structure during in situ biostimulation of subsurface sediment cocontaminated with uranium and nitrate. Appl. Environ. Microbiol. **70:**4911–4920.
33. **Petrie, L., N. N. North, S. L. Dollhopf, D. L. Balkwill, and J. E. Kostka.** 2003. Enumeration and characterization of iron(III)-reducing microbial communities from acidic subsurface sediments contaminated with uranium(VI). Appl. Environ. Microbiol. **69:**7467–7479.
34. **Ren, S. X., G. Fu, X. G. Jiang, R. Zeng, Y. G. Miao, H. Xu, Y. X. Zhang, H. Xiong, G. Lu, L. F. Lu, H. Q. Jiang, J. Jia, Y. F. Tu, J. X. Jiang, W. Y. Gu, Y. Q. Zhang, Z. Cai, H. H. Sheng, H. F. Yin, Y. Zhang, G. F. Zhu, M. Wan, H. L. Huang, Z. Qian, S. Y. Wang, W. Ma, Z. J. Yao, Y. Shen, B. Q. Qiang, Q. C. Xia, X. K. Guo, A. Danchin, I. Saint Girons, R. L. Somerville, Y. M. Wen, M. H. Shi, Z. Chen, J. G. Xu, and G. P. Zhao.** 2003. Unique physiological and pathogenic features of *Leptospira interrogans* revealed by whole-genome sequencing. Nature **422:**888–893.
35. **Roling, W. F., B. M. van Breukelen, M. Braster, M. T. Goeltom, J. Groen, and H. W. van Verseveld.** 2000. Analysis of microbial communities in a landfill leachate polluted aquifer using a new method for anaerobic physiological profiling and 16S rDNA based fingerprinting. Microb. Ecol. **40:**177–188.
36. **Saitou, N., and M. Nei.** 1987. The neighbor-joining method: a new method for reconstructing phylogenetic trees. Mol. Biol. Evol. **4:**406–425.
37. **Salmon, K. A., C. Yang, and G. Wesley Hatfield.** February 2006, posting date. Chapter 3.6.1.5, Biosynthesis and regulation of the branched-chain amino acids *In* R. Curtiss III et al. (ed.), EcoSal—*Escherichia coli* and *Salmonella*: cellular and molecular biology. ASM Press, Washington, DC. http://www.ecosal.org.
38. **Schmidt, K., M. Carlsen, J. Nielsen, and J. Villadsen.** 1997. Modeling isotopomer distributions in biochemical networks using isotopomer mapping matrices. Biotechnol. Bioeng. **55:**831–840.
39. **Segura-Gonzalez, D., R. Mahadevan, K. Juarez-Lopez, and D. R. Lovley.** 2008. Computational and experimental analysis in the central metabolism of *Geobacter sulfurreducens.* PLoS Comput. Biol. 4:e36.
40. **Smith, P. K., R. I. Krohn, G. T. Hermanson, A. K. Mallia, F. H. Gartner, M. D. Provenzano, E. K. Fujimoto, N. M. Goeke, B. J. Olson, and D. C. Klenk.** 1985. Measurement of protein using bicinchoninic acid. Anal. Biochem. **150:**76–85.
41. **Suthers, P. F., A. P. Burgard, M. S. Dasika, F. Nowroozi, S. Van Dien, J. D. Keasling, and C. D. Maranas.** 2007. Metabolic flux elucidation for large-scale models using ^{13}C labeled isotopes. Metab. Eng. **9:**387–405.
42. **Ullmann, R., R. Gross, J. Simon, G. Unden, and A. Kroger.** 2000. Transport of C_4-dicarboxylates in *Wolinella succinogenes*. J. Bacteriol. **182:**5757–5764.
43. **Van Dien, S., T. Strovas, and M. Lidstrom.** 2003. Quantification of central metabolic fluxes in the facultative methylotroph *Methylobacterium extorquens* AM1 using ^{13}C-label tracing and mass spectrometry. Biotechnol. Bioeng. **84:**45–55.
44. **Vrionis, H. A., R. T. Anderson, I. Ortiz-Bernad, K. R. O'Neill, C. T. Resch, A. D. Peacock, R. Dayvault, D. C. White, P. E. Long, and D. R. Lovley.** 2005. Microbiological and geochemical heterogeneity in an in situ uranium bioremediation field site. Appl. Environ. Microbiol. **7:**478–479.
45. **Wiechert, W., C. Siefke, A. A. deGraaf, and A. Marx.** 1997. Bidirectional reaction steps in metabolic networks. 2. Flux estimation and statistical analysis. Biotechnol. Bioeng. **55:**118–135.
46. **Wittmann, C., and E. Heinzle.** 1999. Mass spectrometry for metabolic flux analysis. Biotechnol. Bioeng. **62:**739–750.
47. **Xu, H., Y. Zhang, X. Guo, S. Ren, A. A. Staempfli, J. Chiao, W. Jiang, and G. Zhao.** 2004. Isoleucine biosynthesis in *Leptospira interrogans* serotype lai strain 56601 proceeds via a threonine-independent pathway. J. Bacteriol. **186:**5400–5409.